Variation of Doppler Broadening in High-Temperature Bubbles Created in an ECR Plasma

Atsushi OKAMOTO, Shinji YOSHIMURA[1)], Kenichiro TERASAKA[2)] and Masayoshi Y. TANAKA[2)]

Nagoya University, Nagoya 464-8603, Japan
[1)]*National Institute for Fusion Science, Toki 509-5292, Japan*
[2)]*Kyushu University, Kasuga 816-8580, Japan*

(Received 5 September 2019 / Accepted 28 October 2019)

A high dispersion and high time-resolution spectrometer equipped with two slits in output ports is developed to observe variation of Doppler broadening in the high-temperature bubbles [K. Terasaka, *et. al.*, Phys. Plasmas **25**, 052113 (2018)]. Reduction of Doppler broadening in a line spectrum of helium ion is experimentally observed when the bubbles emerge in the viewing chord of spectrometer. The results suggest possibilities of ion temperature reduction during the high-temperature bubbles.

Keywords: ion temperature, high-temperature bubble, electron cyclotron resonance plasma, Doppler spectroscopy, conditional average

DOI: 10.1585/pfr.14.1201165

High temperature bubbles observed in the electron cyclotron resonance plasmas [1, 2] are localized structure characterized by a few times higher electron temperature compared to the ambient plasma, prolate spheroid along the external magnetic field. The bubbles spontaneously and randomly emerged in the plasma with duration time of the order of microsecond. While variation of the electron temperature has been measured with Langmuir probes and conditional averaging, ion temperature was unclear. In order to understand growth and decay mechanism of the high temperature bubbles, temporal variation of ion temperature will give us essential information on energy balance. Measurement of ion temperature, however, was difficult because of short duration compared with typical exposure time of charge coupled device (CCD) equipped on polychromator.

We have developed a high time-resolution and high dispersion monochromator to resolve Doppler broadening of ion-line emission and have observed temporal variation of Doppler broadening in a plasma with the high temperature bubbles, in which ion temperature reduction in the bubbles are implied.

Experiments were performed in HYPER-I device [3, 4]. Schematic of experimental setup is shown in Fig. 1 (a). Helium plasma was produced by electron cyclotron resonance of 2.45 GHz microwave injected along the magnetic field with the high field side condition. High temperature bubbles were monitored by variation of the floating potential, V_f, at the axis of cylindrical plasma using a Langmuir probe. An optical viewing chord installed along the axis of cylindrical plasma collected line emission of helium ion

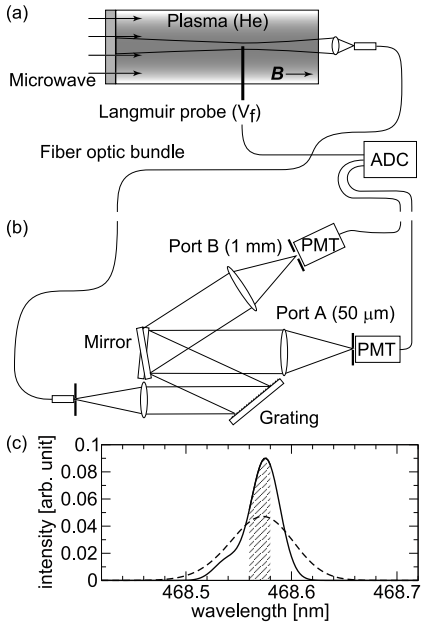

Fig. 1 Schematics of (a) experimental setup in HYPER-I device, (b) spectrometer, (c) calculated spectra considering the fine structure for experimentally determined 53 μm of instrumental width. Shading indicates the slit width of port A. Solid and broken curves correspond to $T_\mathrm{i} = 1$ eV and $T_\mathrm{i} = 11$ eV.

(468.6 nm, $n = 3 - 4$) with the observation spot size of 10 mm in radius, which was transferred to the high time-resolution and high dispersion monochromator through an optical fiber bundle.

As shown in Fig. 1 (b), the monochromator has two

author's e-mail: okamoto.atsushi@nagoya-u.jp

output ports. The line emission injected from an entrance slit (50 μm in width) was collimated through a lens (850 mm in focal length), diffracted by a grating (50 × 50 mm in dimension and 2400 lines/mm in groove density), split to two ports by mirrors, and focused by lenses on different width of exit slits. Reciprocal linear dispersion was 0.43 nm/mm. Port A has a narrow (50 μm width) slit to detect the center part of broadening spectrum as shown in Fig. 1 (c), while port B has a wide (1 mm width) slit to detect whole spectrum. Intensity ratio of port A to port B, which indicates broadening of spectrum excluding variation of emission intensity, reflects ion temperature. For example, the intensity ratios for Fig. 1 (c) are 0.55 for $T_i = 1$ eV and 0.33 for $T_i = 11$ eV.

The emission intensities from port A and B as well as the floating potential were recorded by an analogue to digital converter (ADC) with sampling rate of 10^6 sampling/s. When the microwave input power is $P = 20$ kW, Fig. 2 (a), large negative spikes in floating potential are frequently observed corresponding to the bubbles. When $P = 10$ kW, on the other hand, smaller spikes are observed as shown in Fig. 2 (b). Emissions measured by photomultiplier tubes (PMT) are recorded as randomly coming photon events as shown in Figs. 2 (c) and (d). In the present experiment, 5×10^6 points (5 second) were recorded for each case. 4.5×10^3 photon events were counted in port A for $P = 10$ kW case as the least case.

To obtain variation of emission intensities, conditional averaging was applied; time trace of the emission intensities were converted to histogram of floating potential bins, where the bin width $\Delta V_f = 1.77$ V was the standard deviation of V_f for $P = 10$ kW. Floating potential dependence of photon fluxes and their ratios are shown in Fig. 3. Histogram of photon flux with statistical error, Fig. 3 (b), shows that absolute flux is larger for the case with more bubbles than that with fewer bubbles. Increasing electron density and temperature result in increase of the line emission intensity of helium ion. This is consistent with the higher electron temperature in the bubbles measured by Langmuir probe [1], especially for the range of negative tail, $V_f \leq 10$ V. In the range near the average $V_f \simeq 15$ V, there is still higher emission intensity for $P = 20$ kW case than that for $P = 10$ kW case. This is simply increase of microwave power resulting in increase of the electron density, because the bubble does not exist in the range near the average V_f even for the $P = 20$ kW case.

Intensity ratios are 0.222 ± 0.003 for $P = 20$ kW and 0.169 ± 0.005 for $P = 10$ kW in the most probable (average) V_f bin as shown in Fig. 3 (c). On the other hand, the ratio is higher for the tail region $V_f \leq 10$ V. The result indicates that the spectrum width of the ion emission line sharpen during the high temperature bubbles existing in the viewing chord. While the electron temperature increases in the bubbles, the reduction of ion temperature is implied. Obtaining absolute value of ion temperature requires precise sensitivity calibration with $T_i \simeq 0$ eV ion emission source in addition to instrumental width determination, which will be our future work. It is noted that the statistical error shown in Fig. 3 (c) is $\pm 1\sigma$. Data in $V_f < 5$ V bins for $P = 10$ kW case are omitted due to larger error in the ratio, which is caused by smaller photon flux in port A (narrow slit) and smaller probability of V_f (rare event). Possible mechanisms of the ion temperature reduction in the bubbles are (1) reduction of electron-ion relaxation frequency due to increasing electron temperature and (2) increase in cold ions due to increasing ionization rate. The latter, however, will compete with decreasing charge-exchange rate, which will reduce energy loss from ions to neutrals.

Variation of Doppler broadening during the high temperature bubbles is observed for the first time using a

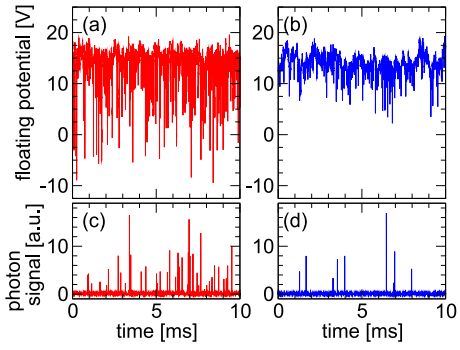

Fig. 2 Typical time trace of (a), (b) floating potential, (c), (d) photon signal detected by the photo-multiplier tube in port A. (a) and (c) correspond to microwave input power $P = 20$ kW, while (b) and (d), $P = 10$ kW.

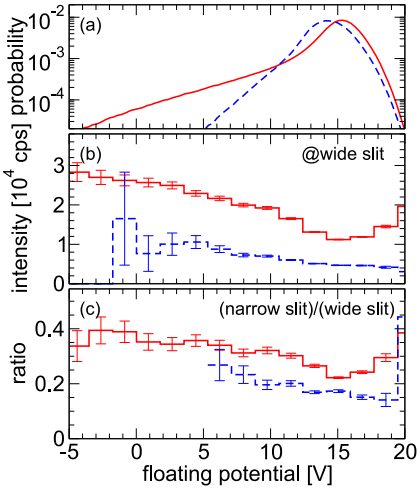

Fig. 3 (a) Probability in floating potential, (b) floating potential dependence of photon flux at the wide slit, and (c) photon flux ratio of narrow slit to wide slit. Solid lines represent the high temperature bubble case with $P = 20$ kW, broken lines smaller and fewer bubbles with $P = 10$ kW.

newly developed high time-resolution and high dispersion monochromator. While detailed understanding remains our future work, the results imply reduction of ion temperature during the bubbles.

This work is performed with the support and under the auspices of the NIFS Collaboration Research Program (NIFS16KBAP029, NIFS18KBAP044).

[1] K. Terasaka *et al.*, Phys. Plasmas **25**, 052113 (2018).
[2] S. Yoshimura *et al.*, Plasma Fusion Res. **10**, 3401028 (2015).
[3] M.Y. Tanaka *et al.*, Rev. Sci. Instrum **69**, 980 (1998).
[4] S. Yoshimura *et al.*, J. Plasma Phys. **81**, 345810204 (2015).